

**Optimizing biologically inspired transport networks by control**Junjie Jiang,<sup>1</sup> Xingang Wang,<sup>2</sup> and Ying-Cheng Lai<sup>1,3,\*</sup><sup>1</sup>*School of Electrical, Computer and Energy Engineering, Arizona State University, Tempe, Arizona 85287, USA*<sup>2</sup>*School of Physics and Information Technology, Shaanxi Normal University, Xi'an 710062, China*<sup>3</sup>*Department of Physics, Arizona State University, Tempe, Arizona 85287, USA*

(Received 20 March 2019; published 20 September 2019)

Transportation networks with intrinsic flow dynamics governed by the Kirchhoff's current law are ubiquitous in natural and engineering systems. There has been recent work on designing optimal transportation networks based on biological principles with the goal to minimize the total dissipation associated with the flow. Despite being biologically inspired, e.g., adaptive network design based on slime mold *Physarum polycephalum*, such methods generally lead to suboptimal networks due to the difficulty in finding a global or nearly global optimum of the nonconvex optimization function. Here we articulate a design paradigm that combines engineering control and biological principles to realize optimal transportation networks. In particular, we show how small control signals applied only to a fraction of edges in an adaptive network can lead to solutions that are far more optimal than those based solely on biological principles. We also demonstrate that control signals, if not properly designed, can lead to networks that are less optimal. Incorporating control principle into biology-based optimal network design has broad applications not only in biomedical science and engineering but also in other disciplines such as civil engineering for designing resilient infrastructure systems.

DOI: [10.1103/PhysRevE.100.032309](https://doi.org/10.1103/PhysRevE.100.032309)**I. INTRODUCTION**

The functioning of a modern society relies on effective transportation networks. To design and optimize such networks with high efficiency and robustness is a significant but extremely challenging problem. For example, as international exchanges of population and goods intensify, the demand to design efficient and robust transportation networks [1,2] is becoming increasingly high. With advancement of urbanization in developing countries, there is an ever growing need for optimal urban transportation networks [3,4]. With the tremendous population growth in many metropolitan areas in the world, how to design highly efficient water distribution networks [5–8] and power grids that are susceptible to cascading failures [9,10] becomes critical in infrastructure, sustainability, and electrical engineering. Traditionally, one aimed to design optimal transportation network by maximizing the transport efficiency at a fixed cost, and there were mathematical results that the topology of an optimal network depends on the convexity of the cost function [11,12]. Later, it was shown [13] that minimizing the dissipation rate under a global constraint is equivalent to minimizing the cost function [11]. The mathematical underpinning of these studies is the principle of Lagrange multipliers, which typically yields only local minima of the cost function. To attain a global minimum has thus been a critical issue. In this regard, a mathematical proof exists that, subject to a global constraint, the optimal transportation network should have a treelike and loopless structure [14]. However, if there are fluctuations in the source and/or sink or if the transport edges are damaged, then loops can appear in the optimal network structure [15,16]. Recently,

global resilience of optimal transportation network in response to failures has been investigated [17,18]. In designing optimal transportation networks subject to global constraints, the principle of Lagrange multipliers is in fact the golden standard.

In natural and especially biological systems, networks that transport energy, chemicals, nutrients, or materials are ubiquitous [19–21]. Examples include leaf veins of plants that deliver and spread nutrients, vascular systems of animals that carry oxygen to the whole body through blood circulation, and river networks that govern the flow of water in certain geographical regions [7,22–24]. Such “nature-designed” networks in general function well in terms of minimizing the “cost” or dissipation and maximizing transport efficiency with reasonable fault tolerance [25]. It is of general interest to design optimal transportation networks as inspired by natural or biological principles. In this regard, there was a method aimed at minimizing the global energy dissipation [26]. A model of adaptive dynamics was articulated [27] for designing optimal transportation networks inspired by slime mold *Physarum polycephalum*, which was based on a positive feedback between the fluxes of nutrients through and the conductivity of the tubes of the biological organism. Especially, the conductivity of a tube (an edge) will increase with the nutrient flux through it and, when the flux is terminated, the conductivity will decrease exponentially to zero. The adaptive-dynamics-based design method is a self-organized process without any centralized control and explicit global information, with the underlying process being to enhance the existing strong tubes and degrade the redundant edges in the network. During the process, the global energy dissipation is minimized. The design principle based on locally adaptive dynamics was used in designing the Tokyo rail system [26] and the major transport networks in Mexico and China [28].

\*Ying-Cheng.Lai@asu.edu

When there are strong fluctuations in the flow distribution, the adaptive-dynamics-based approach tends to generate optimal networks with a hierarchical loop structure [29].

While mother nature always gives us the best possible and most optimal design, because of the structural and dynamical complexities of these networks, it is often difficult to fully comprehend and grasp the underlying design principles. One at best can only hope to have an approximate understanding of these principles. In fact, the biologically inspired adaptive dynamics approach has drawbacks. For example, while ideally one would hope to generate networks according to the global minimum of some cost or energy function, the optimal transportation network structure designed based on adaptive dynamics [26] is the result of reaching only a local minimum of the cost function. A recent work [30] has revealed that adaptive dynamics coupled with the growth of the underlying biological tissue can drive the system to transportation network structure with nearly global optimum (NGO). Mathematically, the biological growth effect can be modeled by a time-dependent, increasing term in the equations underlying the adaptive dynamics. While incorporating a growth mechanism into the network optimizing process has fundamental biological support, there are natural or engineering systems in which growth is not important, such as water transport networks. An interesting question is then whether NGO transportation networks based on adaptive dynamics can be designed without any growth mechanism.

In this paper, we articulate and investigate the principle of incorporating control into adaptive dynamical evolution to arrive at NGO transportation networks without the need to impose any growth mechanism. The basic idea is schematically illustrated in Fig. 1. Specifically, we randomly choose a set of edges and add control signals to the equations governing their adaptive dynamical evolution. The system will then evolve into one with a hierarchical structure with high total dissipation  $E$ , as shown on the right side of Fig. 1(a). A suitable control signal can remove the hierarchical structure so as to reduce the total dissipation. Extensive control, e.g., controlling all edges, can lead to an NGO transportation network, as shown on the left side of Fig. 1(a). However, the scheme to apply a control signal to each and every edge in the network may be unrealistic. We find that a temporal control strategy in which a random, time-dependent subset of edges are chosen to be controlled in every fixed time interval, as shown in Fig. 1(b), can be advantageous. Although only a small fraction of the edges are subject to control in any given time interval, the end result is an NGO transportation network after a long time evolution. Variations in the control such as targeting the edges with relatively small values of conductivity can also lead to an NGO network solution, as shown in Fig. 1(c). Extensive computations show that diverse strategies to control locally adaptive dynamics can in general achieve the goal of generating an NGO transportation network. Thus, while it is extremely difficult to find an exact global minimum of the complex nonconvex cost function, realistic but nontrivial control can lead to transportation networks corresponding to solutions as close to the global minimum as possible. We note that, biologically, for an organism such as *P. polycephalum* [31], the control signal could be time-dependent light illumination. While the manifestation of the control signal depends

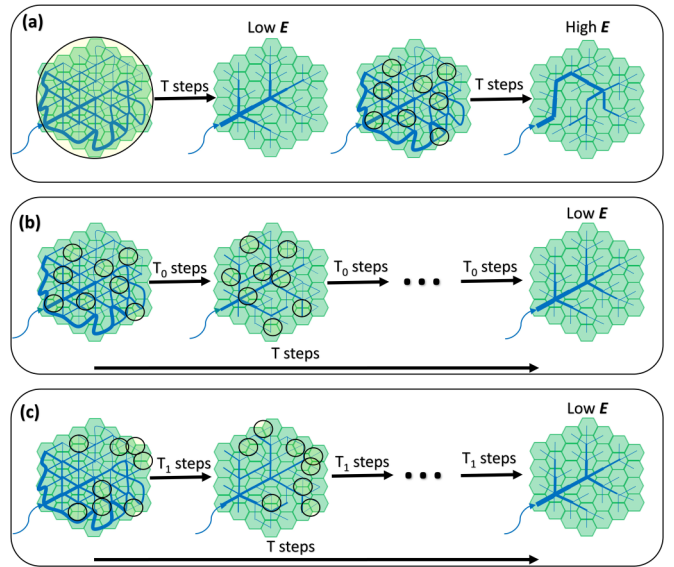


FIG. 1. Controlling adaptive dynamics to generate nearly optimal transportation network structure. For different control strategies, the effects are different. The green surface illustrates the underlying “tissue” and the blue lines represent the connected tubes. The total dissipation of the transportation network is  $E$ . The edges within the black circles are controlled ones. (a) Strategy example 1: A control signal is applied to every edge. After evolving the adaptive dynamics for a long time, a nearly optimal network structure with low total dissipation emerges, as indicated by the two left panels. However, if control signals are added to only a small subset of randomly chosen edges, then the resulting network will possess high total dissipation, as demonstrated by the two right panels. (b) Strategy example 2: Temporal control where a varying, random subset of edges receive control signals every certain time interval. This strategy can lead to a nearly globally optimal transportation network structure. (c) Strategy example 3: Applying temporal control signals to a subset of edges with small conductivity. In this case, the final network can also be nearly globally optimal.

on the specific context, letting it be a power grid, a network of water transportation channels, or a public transportation network, our work demonstrates that flexible control strategies can lead to the most optimal possible of such networks, providing the designers with more options and a greater level of freedom.

We note that an alternative global minimization method has been articulated and studied, one based on simulated annealing [15], which can generate NGO transportation networks with a highly symmetric hierarchical structure and dense connections. However, the method is computationally intensive and the final solution depends sensitively on the initial condition. In comparison, our method is computationally efficient and robust.

## II. ADAPTIVE NETWORK DYNAMICS AND CONTROL FORMULATION

### A. Adaptive dynamics

We consider networks that evolve adaptively in a bounded, two-dimensional region (a sheet). The sheet can represent

a tree leaf, a river basin, the power grid or a water supply network in a city. Initially, we place a mesh on the sheet as a triangular lattice or Voronoi tessellation. The coarse-grained network has  $n$  tessellation units and  $m$  edges among them. Let  $Q_l$  be the flux through edge  $l$ , which is defined as

$$Q_l = \kappa_l \frac{P_i - P_j}{D_l}, \quad (1)$$

where  $\kappa_l$  and  $D_l$  are the conductivity and Euclidean distance of the edge between units  $i$  and  $j$ ,  $P_i$ , and  $P_j$  denote the potential at unit  $i$  and  $j$ , respectively. For laminar flow transport in the coarse-grained network, the Poiseuille's law gives that the conductivity of the edge connecting units  $i$  and  $j$  is  $\kappa_{ij} = \pi r^4 / 8\eta$ , where  $r$  is the radius of the tube and  $\eta$  is the fluid viscosity. The flow vector  $\mathbf{Q}$  is defined as

$$\mathbf{Q} = \kappa \cdot \mathcal{D}^{-1} \cdot \mathcal{A} \cdot \mathbf{P}, \quad (2)$$

where  $\mathcal{D}$  and  $\kappa$  are the diagonal matrices of the edge distance and conductivity, respectively,  $\mathbf{P}$  is the vector of potential of all the units, and  $\mathcal{A}$  is the  $m \times n$  incidence matrix of the coarse-grained network with the property that the sum of all elements in any row is zero. Each row of matrix  $\mathcal{A}$  contains two nontrivial elements only: a 1 and a  $-1$ , corresponding to one edge in the coarse-grained network, and all other elements are 0. The Kirchhoff's current law stipulates that the balanced flow in each unit can be calculated as

$$\mathcal{A}^T \cdot \mathbf{Q} = \mathbf{I}, \quad (3)$$

where  $\mathcal{A}^T$  is the transpose of the incidence matrix and  $\mathbf{I}$  is a vector specifying whether there is a source or a sink at each unit. In plant biology, the  $i$ th element  $I_i$  of the vector  $\mathbf{I}$  records the sap input into the  $i$ th unit or its usage. It is convenient to set  $I_s = I_0$  for a source unit and  $I_u = I_0 / (n - 1)$  for a usage unit. For simplicity, we assume that the network has only one source unit, while all other units are sinks. The vector  $\mathbf{I}$  is given by

$$\mathbf{I} = [-I_0 / (n - 1), \dots, -I_0 / (n - 1), I_0, -I_0 / (n - 1), \dots, -I_0 / (n - 1)]^T.$$

Combining Eqs. (2) and (3), we get the following relationship between  $\mathbf{P}$  and  $\mathbf{I}$ :

$$\mathcal{A}^T \cdot \kappa \cdot \mathcal{D}^{-1} \cdot \mathcal{A} \cdot \mathbf{P} = \mathbf{I}, \quad (4)$$

with the solution given by

$$\mathbf{P} = (\mathcal{A}^T \cdot \kappa \mathcal{D}^{-1} \cdot \mathcal{A})^\dagger \cdot \mathbf{I}, \quad (5)$$

where  $\dagger$  represents the Moore-Penrose pseudoinverse. With the solution of  $\mathbf{P}$  by  $\mathbf{I}$ , substituting Eq. (5) into Eq. (2), we obtain the dependence of the balanced flow  $\mathbf{Q}$  on  $\mathbf{I}$  and  $\kappa$  as

$$\mathbf{Q} = \kappa \cdot \mathcal{D}^{-1} \cdot \mathcal{A} \cdot (\mathcal{A}^T \cdot \kappa \cdot \mathcal{D}^{-1} \cdot \mathcal{A})^\dagger \cdot \mathbf{I}. \quad (6)$$

Experimentally, it was observed that, in *P. polycephalum*, there is a positive feedback between the flux and conductivity of an edge [26]. This means that a large flux will increase the conductivity of the edge. However, a small flux will gradually degenerate the edge. In general, the positive feedback mechanism alone is unable to evolve the system into an NGO transportation network.

## B. Formulation of control

To incorporate control into the dynamical evolution to obtain an NGO solution of the final network, we assume that the conductivity  $\kappa_l$  depends not only on the flux  $Q_l$  but also on the control signal  $g(t, \mu)$ :

$$\frac{d\kappa_l}{dt} = f(|Q_l|) - \kappa_l + \delta_{lc} g(t, \mu), \quad (7)$$

where  $|Q_l|$  is the absolute value of flux  $Q_l$  and  $c$  is an edge belonging to the set  $C$  in which there is a control signal added to the adaptive dynamical evolution equation of each edge. If edge  $l$  belongs to  $C$ , then  $\delta_{lc} = 1$ ; otherwise,  $\delta_{lc} = 0$ . The first term  $f(|Q_l|)$  in Eq. (7) is the positive feedback between the flux and conductivity of edge  $l$ . In a previous study [26], two types of forms of  $f$  were considered. The first one is  $f(|Q_l|) = (|Q_l|)^\nu$ . The second form takes into account the saturation effect:  $f(|Q_l|) = |Q_l|^\nu / (1 + h|Q_l|^\nu)$ , where  $h$  is the half-saturation constant. In our work, we use the second form of  $f$ , but we have verified that implementing the first form yields qualitatively similar results.

We choose the control function  $g(t, \mu)$  to be a sigmoid function (a Fermi-Dirac distribution like function), defined as

$$g(t, \mu) = \frac{1}{1 + e^{(t-\mu)/\sigma}}, \quad (8)$$

where  $\mu$  and  $\sigma$  are parameters. The value of  $\mu$  determines when the control signal will change the edge conductance, where a larger value of  $\mu$  will lead to a longer delay in the effect of the control signal. The parameter  $\sigma$  is the decay rate of the control signal with time. This form of the control signal is inspired by the growth mechanism in transportation network design [30]. The basic requirement of the control signal is that it gradually approaches zero from a positive value. To be concrete, we consider three methods to choose the control set  $C$ : (1) random choice of the control edges, (2) choosing edges with small conductivity, and (3) choosing edges with large conductivity. Our general control strategy is to add a control signal to each node in the control set  $C$  every  $T_0$  time steps, as illustrated in Fig. 1(b). For one realization, we fix a method to choose the control set and, for a different time interval of  $T_0$  steps, a different control set is chosen. The control signal  $g(t, \mu)$  is time dependent, but it does not depend on the specific control set  $C$ . Associated with our control strategy, there are two limiting situations. The first one is that the control set  $C$  changes every time step ( $T_0 = 1$ ). The second is a fixed control set:  $T_0 = +\infty$ .

## C. Total dissipation and cost constraint

We aim to find the network structure that minimizes the total dissipation of the transportation process subject to the cost constraint. For any edge, the dissipation is determined by the flux through and conductivity of the edge: a larger flux and smaller conductivity lead to higher dissipation while a smaller flux and larger conductivity give rise to weaker dissipation. It would thus seem that edges with larger conductivity are preferred. However, this is practically difficult due to the cost constraint. Previously, it was proved [13] that for a concave cost constraint, the optimization process leads to networks that

are realistic and feasible (e.g., without requiring arbitrarily large conductivity).

In general, the total dissipation of the network can be defined as

$$E = \sum_l D_l \frac{Q_l^2}{\kappa_l}, \quad (9)$$

and the cost constraint is

$$\sum_l D_l \kappa_l^\beta \equiv \text{const}, \quad (10)$$

where  $\beta \in (0, 1)$  is the cost limiting parameter. In a general sense, the cost constraint is the result of the finite amount of material available to construct the physical network [15,16,29]. In order to generate physically realizable networks, we demand that the cost function be concave [13]. For such a choice, it is possible for adaptive dynamical evolution to minimize the total dissipation  $E$ . Incorporating the cost constraint into the control framework enables us to generate NGO transportation networks.

#### D. Dynamical evolution process

We solve the adaptive dynamical equation using the unit time step, together with the flow balance equation. The conductivity obtained directly from the solution is in general not consistent with the cost constraint. A previous approach exploited the method of Lagrange multiplier to generate the desired conductivity value [32]. However, this approach will cause unjustified changes in the network structure. We thus exploit the simple method of rescaling the conductivity. In particular, from  $\hat{\kappa}_l$ , the original conductivity of edge  $l$  obtained from the solution of the adaptive equation, the rescaled conductivity is given by

$$\kappa_l = \left( \frac{\text{const}}{\sum_l D_l \hat{\kappa}_l^\beta} \right)^{1/\beta} \hat{\kappa}_l, \quad (11)$$

where const is the cost constraint. The evolution process is then governed by two equations:

$$\begin{aligned} \mathbf{Q} &= \kappa \cdot \mathcal{D}^{-1} \cdot \mathcal{A} \cdot (\mathcal{A}^T \cdot \kappa \cdot \mathcal{D}^{-1} \cdot \mathcal{A})^\dagger \cdot \mathbf{I}, \\ \frac{d\hat{\kappa}_l}{dt} &= f(|Q_l|) - \hat{\kappa}_l + \delta_{lc} g(t, \mu), \end{aligned} \quad (12)$$

where the flux  $\mathbf{Q}$  is calculated from the controlled adaptive dynamics with the normalized conductivity. While convenient, conductivity normalization is not necessary for realizing an NGO transportation network. As Eqs. (6) and (2) show, flow in an edge is not affected by normalization even though the normalization can affect the potential on a unit. In our simulations, we set the parameters as  $I_0 = 1$ ,  $\beta = 1/2$ ,  $\gamma = 4/3$  and initial conductivity value  $\kappa_l = \kappa_0 = 1/2$ . Note that  $D_l$  is the Euclidean length of edge  $l$ , which depends on the lattice structure or Voronoi tessellation.

The main goal of our work is to generate from a coarse-grained network of  $n$  tessellation units and  $m$  edges NGO transportation networks that minimize the total dissipation [Eq. (9)] subject to the cost constraint [Eq. (10)]. In the coarse-grained network, there are 1 source and  $n - 1$  sink units. The optimization process follows the biologically inspired

adaptive equation with control, as described in Eq. (12). The evolution of the adaptive equation decreases the total dissipation of the designed transportation network gradually and the total cost based on the normalization process in Eq. (11). When a suitable control signal [Eq. (8)] is applied to certain edges, an NGO transportation network emerges.

The protocol to arrive at an optimal transportation network can then be described, as follows. One starts by generating a coarse-grained network, where every edge has the same initial conductance. Based on the initial conductance and the Euclidean distance of every edge, one calculates the cost constant using Eq. (10). One then evolves the biologically inspired adaptive dynamics as in Eq. (12), from which the flow matrix  $\mathbf{Q}$  and the relative conductance  $\hat{\kappa}$  of every edge that depends on the flow can be calculated. After obtaining the relative conductance  $\hat{\kappa}$ , one uses Eq. (11) to normalize it to generate the constrained conductance  $\kappa$ . Finally, one repeats this process until an NGO transportation network has emerged, as signified by the minimization of the total dissipation by the constrained conductance  $\kappa$ .

### III. RESULTS

#### A. Effect of global control: Emergence of NGO network structure with minimum dissipation

In the absence of control, the adaptive dynamical evolution is unable to drive the network to one with an NGO structure, but control can result in an NGO network, as shown in Fig. 2. In particular, we begin with a two-dimensional tissue of a hexagon shape, which is a combination of two identical triangular lattices, one displaced with respect to the other. Each triangular lattice has 217 units and 600 edges. Without control, the final optimal network structure from the adaptive dynamical evolution contains no hierarchical structure, as shown in Fig. 2(a). The network structure corresponds to a local minimum of total dissipation:  $E \approx 0.075$ , as shown in Fig. 2(c). When a suitable control signal is applied to each and every edge in the network, an NGO transportation network with a hierarchical structure emerges, where the control signal is  $1/[1 + e^{(t-250)/50}]$ . As shown in Fig. 2(b), the NGO network resembles in structure the vein network of a leaf of some natural plant. The evolution of the total dissipation is shown in Fig. 2(d), where the total dissipation is  $E \approx 0.045$ , representing a 40% reduction in the total dissipation with respect to the case without control. Comparing Figs. 2(c) with 2(d), we see that, initially, the total dissipation is lower for the adaptive dynamics without control, but in this case the network structure cannot evolve to one with an NGO structure. A global control signal applied to all edges makes the emergence of an NGO structure possible.

#### B. Effect of partial control: Nonmonotonic behavior in dissipation

While a unique NGO transportation network can be obtained by controlling all edges in the network, realistically only a fraction of the edges are accessible to control, especially for large systems. It is of practical interest to investigate the possibility of generating NGO transportation networks through partial control.

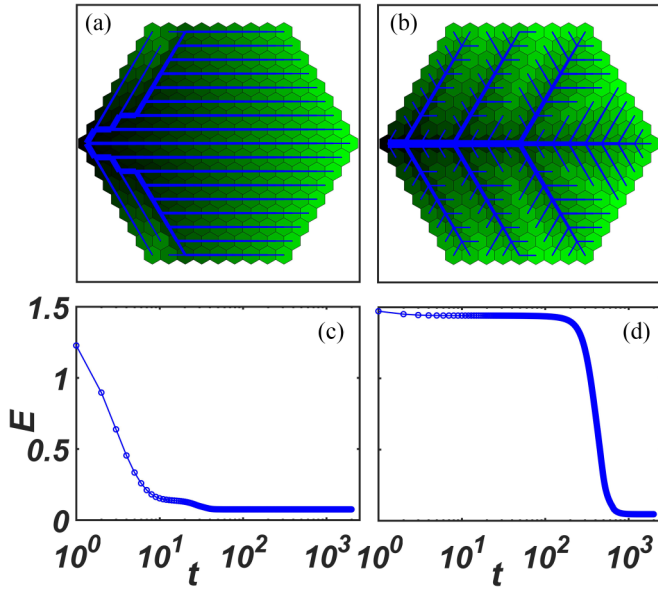


FIG. 2. Resulting optimal network structure without and with control. [(a) and (b)] Optimal transportation network structure resulted from the evolution of adaptive dynamics without and with control, respectively. Edges with conductivity value less than  $10^{-8}$  are not shown. [(c) and (d)] Time evolution of the total dissipation without and with control, respectively. The small hexagons denote lattice units in (a) and (b). The green color represents the value of the potential in the unit, where a brighter color indicates a lower potential value. The width of a blue edge is proportional to  $\kappa^{1/4}$  in (a) and (b). All edges are subject to control. The optimal transportation networks in panels (a) and (b) have total dissipation  $E = 0.074977$  and  $E = 0.045287$ , respectively. The parameters are  $h = 0.001$ ,  $n = 217$ ,  $m = 600$ ,  $\beta = 1/2$ , and  $T = 2000$ . The parameter values for the control signal are  $\mu = 250$  and  $\sigma = 50$ . A movie showing the continuous evolution of the transportation network structure with control is provided as Supplemental Material Video 1 [33].

For partial control where an external signal is added to a fraction  $r$  of randomly chosen edges in a triangular lattice, we first calculate the total dissipation  $E$ . Representative resulting networks for four different values of  $r$  are shown in Fig. 3(a), while the ensemble averaged value of  $E$  versus  $r$  is shown in Fig. 3(b). Intuitively, one may expect that, as the fraction of controlled edges is increased, the total dissipation would decrease monotonically. However, the result in Fig. 3(b) indicates a nonmonotonic behavior, where the dissipation starts to increase as the value of  $r$  is increased from zero, reaches a maximum value, and then decreases with  $r$ . The network corresponding to the maximum dissipation has the structure of a distorted main vein of considerable length, as shown in Fig. 3(a) for the case of  $r = 0.32$ . It is the long vein which results in the high dissipation, even though the transportation network has a hierarchical structure. The general observation is that, if partial control is not strong enough in the sense that the fraction of controlled edges is not sufficiently large, control is detrimental to realizing an optimal network with low dissipation. Note that, for a given value of  $r$ , there are many different choices of the subset of edges for control, leading to statistical fluctuations in the total dissipation, as shown in Fig. 3(b). The variance of the fluctuations increases

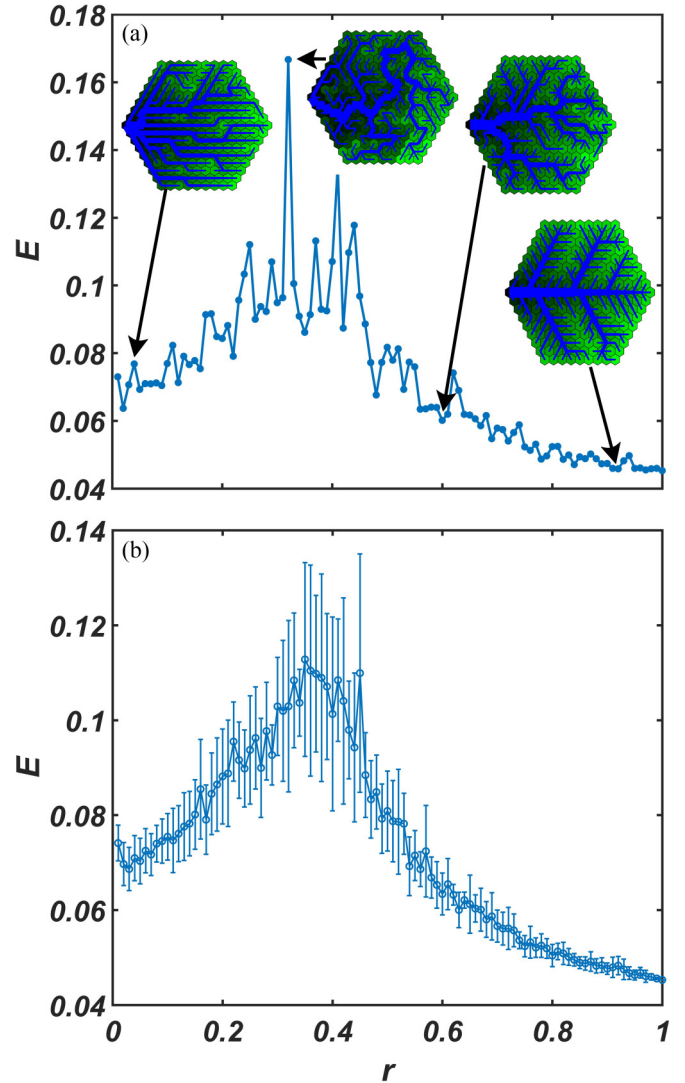


FIG. 3. Nonmonotonic behavior in total dissipation associated with partial control. When a control signal is applied to a subset of edges (partial control), the total dissipation in the long time limit exhibits a counterintuitive, nonmonotonic behavior with the fraction of controlled edges. (a) A single realization of the total dissipation  $E$ , where four representative transportation networks resulted from four different  $r$  values are illustrated. The network structure from left to right corresponds to  $r = 0.04$ ,  $0.32$ ,  $0.6$ , and  $0.92$ , respectively. (b) Ensemble averaged value of the total dissipation  $E$  versus  $r$ , where the ensemble size is 10. The control signal is  $1/[1 + e^{(r-250)/50}]$ . The set of controlled edges is fixed. All other parameter values are the same as in Fig. 2. The transportation networks emerged from partial control with systematically increasing values of  $r$  are shown in Supplemental Material Video 2 [33].

with the amount of the dissipation. For  $r \lesssim 1$ , the total dissipation reaches minimum and the variances tend to zero. (A detailed discussion of the nonmonotonic behavior is given in Sec. IV B.)

We test two alternative partial control strategies that target the edges with small and large conductivity values, respectively, with results shown in Fig. 4. When partially controlling the small conductivity edges, a nonmonotonic behavior

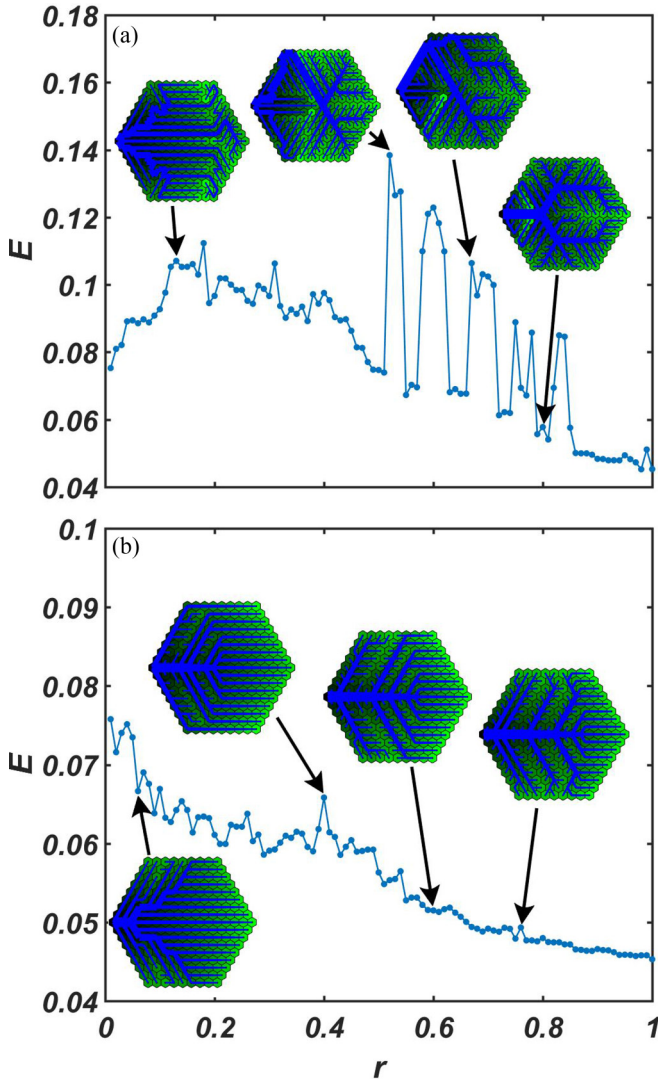


FIG. 4. Total dissipation of transportation network as a result of selective control. Two selective strategies are tested: one controlling edges with small and another with large conductivity. (a) Total dissipation versus the fraction of controlled edges with the lowest possible conductivity values, together with four representative network structures for  $r = 0.13$ ,  $r = 0.52$ ,  $r = 0.67$ , and  $r = 0.8$  (from left to right, respectively). (b) Total dissipation versus the fraction of controlled edges with the highest possible conductivity values, together with four representative network structures for  $r = 0.06$ ,  $r = 0.4$ ,  $r = 0.6$ , and  $r = 0.76$  (from left to right, respectively). The control signal is the same as that in Fig. 3. Since initially, all edges are set with the same conductivity value, we differentiate the edge conductivity after the first time step. The set of controlled edges is fixed. All other parameters have the same values as in Fig. 2.

between the total dissipation and the fraction of the controlled edges still occurs, as shown in Fig. 4(a). However, the transportation network structure with the highest total dissipation does not possess the structure of a main vein. For  $r \in [0.5, 0.9]$ , there are a number of peaks in the total dissipation with a similar structure for the underlying networks. The networks for  $r = 0.52$  and  $r = 0.67$  both have a main but folded vein, where the folds increase the length of the main vein and result in higher dissipation. In the opposite case

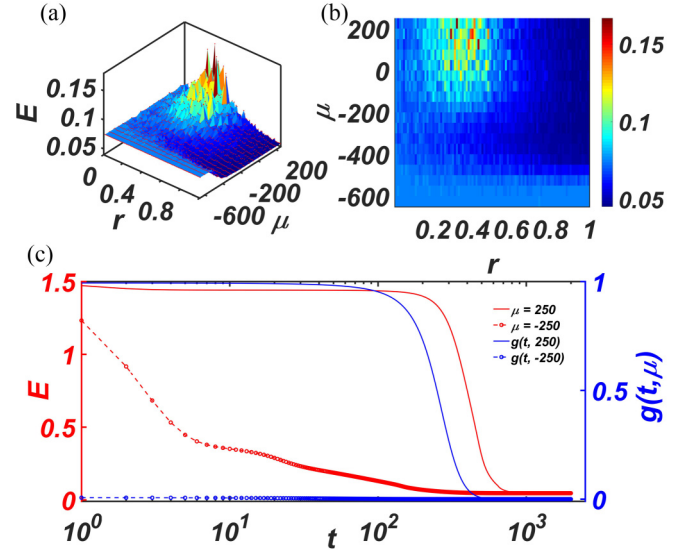


FIG. 5. Phase diagram of total dissipation in a representative parameter plane. [(a) and (b)] Two different views of the parameter plane  $(r, \mu)$ , where  $r$  is the fraction of randomly chosen edges subject to control and  $\mu$  is a parameter characterizing the control signal. The base lattice system from which the network evolves is the two-dimensional hexagonal tissue in Fig. 2. The small red dots in (a) are the numerically calculated values. Due to the high computational load, a single realization of the evolution process is used to generate the phase diagram. However, as shown in Fig. 3, the fluctuations are small in comparison with the value of the total dissipation itself. (c) Time evolution of the total dissipation (red, ordinate on the left side) and the corresponding control signals (blue, right side ordinate) for two points in the phase diagram. The solid and dashed curves correspond to  $(r = 1, \mu = 250)$  and  $(r = 1, \mu = -250)$ , respectively. The set of controlled edges is fixed. Other parameter values are the same as those in Fig. 2.

of partially controlling edges with large conductivity values, the total dissipation versus the fraction of controlled edges exhibits an approximately monotonic behavior, as shown in Fig. 4(b). As more such edges are controlled, the hierarchical structure in the network becomes more pronounced.

### C. Effect of partial control: NGO network structure and varying control signal

The abnormal increase in the total dissipation with the fraction of controlled edges, as exemplified in Fig. 3, is undesirable, as the control fails to realize the intended goal of reducing the dissipation and generating a diverse set of NGO transportation networks. Figure 5 presents a phase diagram of the total dissipation in the parameter plane  $(r, \mu)$ , where  $r$  is the fraction of randomly chosen edges subject to control and  $\mu$  is a parameter characterizing the control signal. We see that choosing a different control signal can remove the undesired behavior. For example, the abnormal increase in the total dissipation occurs for  $\mu \gtrsim -150$ . Choosing  $\mu \lesssim -150$  will then remove the behavior. However, if the value of  $\mu$  is too small, the effect of control will diminish. Empirically, for the parameter setting in Fig. 5, a viable range for the value of  $\mu$  is  $\mu \in (-350, -150)$  for  $\sigma = 50$ , where the dissipation

decreases monotonically as more edges are subject to control and a diverse set of NGO transportation networks can be generated through partial control. Figure 5(c) shows the time evolution of the total dissipation and the underlying control signals for  $\mu = -250$  and  $\mu = 250$ , where the signal for the former  $[g(t, -250)]$  is much weaker than the latter  $[g(t, 250)]$ . The two control signals lead to similar NGO networks, but the number of the time steps required to achieve the NGO solution for the former is less than that for the latter. It is of practical interest to investigate whether a diverse set of NGO transportation networks can be generated through partial control.

#### D. Effect of varying control switching time interval

In our control method, a fraction  $r$  of edges are randomly selected during each time interval  $T_0$ . We find that, reducing the value of  $T_0$  so as to make the set of controlled edges change more frequently can lead to NGO networks with small value of  $r$ , as shown in Figs. 6(a) and 6(b). For example, Fig. 6(a) shows, for  $\mu = 250$ , the emergence of an NGO network when 50% of the edges are subject to control and the set of controlled edges switches every 10 time steps. However, if the value of  $T_0$  is larger, e.g.,  $T_0 = 1000$ , then the total dissipation will still exhibit a nonmonotonic behavior with  $r$ . A similar behavior occurs for  $\mu = -250$ , where the desired switching time interval is  $T_0 < 100$ , as shown in Fig. 6(b). When specifically targeting edges with relatively small or large conductivity values, we obtain similar results, as shown in Figs. 6(c)–6(f), with the feature that rapid switching of the set of controlled edges is more effective if these edges have small conductivity values.

#### E. Effect of positive feedback parameter $\gamma$

Here we studied how different values of the positive feedback parameter  $\gamma$  affect the total dissipation of the controlled adaptive dynamics. Figure 7 shows the total dissipation versus  $\gamma$ , with three specific examples of the resulting NGO network. For  $\gamma \approx 4/3$ , the total dissipation reaches a minimum. A discontinuous change in the total dissipation occurs between  $\gamma = 1$  and  $\gamma = 1.02$ , due to a characteristic difference in the structure of the resulting network. In particular, for  $\gamma = 1$ , the network has a structure with more uniformly distributed conductivity, while the transportation network for  $\gamma = 1.02$  has a main vein structure. For  $\gamma = 2$ , the dissipation is high because the final network has a hierarchical structure with a relatively long main vein with a high conductivity value, so the conductivity values of the edges between the main vein and the sink units are small.

### IV. THEORETICAL INSIGHTS

In the field of optimal transportation network design, previous results were mostly numerical [14,26–29], as it is not feasible to develop an analytic theory to understand the adaptive dynamical processes leading to NGO transportation networks. When control is present, analysis becomes even more difficult. Nonetheless, theoretical insights into certain aspects of the adaptive dynamics subject to control can be gained through a physical analysis.

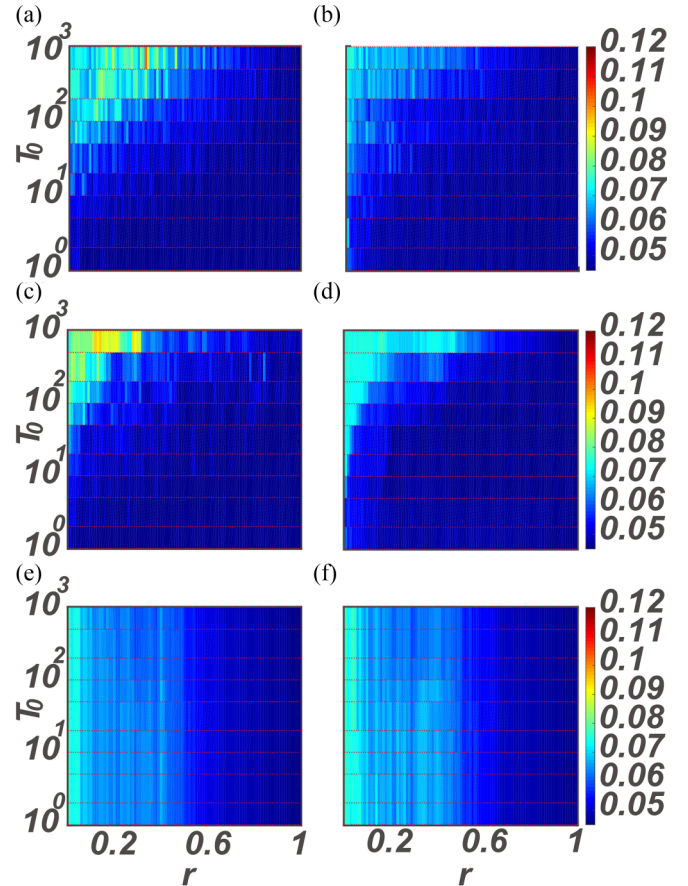


FIG. 6. Phase diagrams of total dissipation in the  $(r, T_0)$  parameter plane. [(a) and (b)] Controlling a randomly selected set of edges, [(c) and (d)] controlling a set of targeted edges with small conductivity, and [(e) and (f)] controlling a set of targeted edges with large conductivity. Panels in the left (right) columns correspond to  $\mu = 250$  and  $\mu = -250$ , respectively. Legends are the same as those in Fig. 5. Other parameters are  $\sigma = 50$ ,  $T = 5000$ . For  $T_0 = 10$  and  $\mu = -250$ , the resulting transportation networks for different values of  $r$  are shown in Supplemental Material Video 3 [33]. The resulting networks by targeting  $r$  fraction of edges with small conductivity values for  $(T_0 = 1, \mu = 250)$  and  $(T_0 = 10, \mu = -250)$  are shown in Supplemental Material Videos 4 and 5, respectively [33]. The results show that controlling the smallest conductance edge is better than controlling the largest conductance edge or a randomly picked edge, indicating the possible critical role played by the small-conductance edges.

#### A. Scaling law between flow and conductance

Previously, it was proved that, under a global constraint, where adaptive dynamics lead to optimal transportation networks with a treelike, loopless topology [14], an optimal flow scaling law exists for this kind of systems [8,34]. Scaling laws between flow and conductance for both homogeneous and disordered transportation networks were also studied [35]. Numerically, we find that, when control is present, the NGO transportation networks possess a hierarchical, treelike structure. To gain theoretical insights, it is useful to derive the scaling law between flow and conductance in the presence of control.

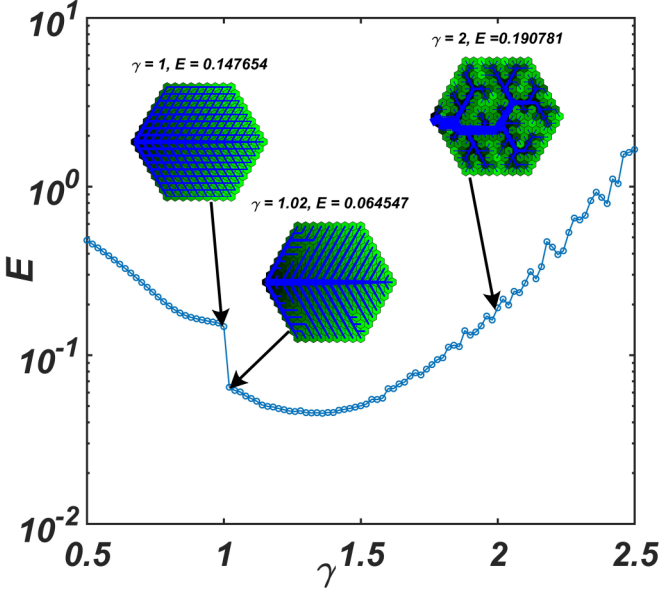


FIG. 7. Effect of positive feedback parameter  $\gamma$  on NGO network. The control scheme is to apply an external signal to 50% of the edges with small conductivity for  $T_1 = 10$  and  $\mu = 250$ . The three networks shown obtained after 2000 time steps are for  $\gamma = 1$ ,  $\gamma = 1.02$ ,  $\gamma = 2$  (from left to right). Other parameters are the same as those in Fig. 2.

Say the coarse-grained network of the underlying tissue has  $n$  tessellation units and  $m$  edges between them. The NGO transportation network has  $n - 1$  edges, as shown in Fig. 2. Without or with control, a similar algebraic scaling relation between the flow through an edge and its conductivity value arises, as shown in Fig. 8. In the three cases demonstrated, the algebraic scaling exponent  $1/\gamma$  exhibits the same approximate value of 0.75. For edge  $l$  edge, we can thus write  $\ln(|Q_l|) = a \ln(\kappa_l) + b$ , where  $a = 1/\gamma$  and  $b$  is an undetermined constant.

We first consider the case of  $f(|Q_l|) = (|Q_l|)^\gamma$ . For  $t \rightarrow \infty$ , we have  $g(t, \mu) \rightarrow 0$ . When the adaptive dynamics have reached a steady state, we have

$$(|Q_l|)^\gamma - \hat{\kappa}_l = 0. \quad (13)$$

Substituting the flow-conductivity scaling relation into Eq. (13), we obtain

$$[e^b(\kappa_l^{1/\gamma})]^\gamma - \hat{\kappa}_l = 0, \quad (14)$$

so the relationship between  $\kappa_l$  and  $\hat{\kappa}_l$  can be written as

$$\kappa_l = \left( \frac{\text{const}}{\sum_l D_l \hat{\kappa}_l^\beta} \right)^{1/\beta} \hat{\kappa}_l. \quad (15)$$

Setting  $\lambda = \text{const}/\sum_l D_l \hat{\kappa}_l^\beta$ , we have  $\kappa_l = \lambda^{1/\beta} \hat{\kappa}_l$ . Substituting this into Eq. (14) yields

$$\{e^b[(\lambda^{1/\beta} \hat{\kappa}_l)^{1/\gamma}]\}^\gamma - \hat{\kappa}_l = 0. \quad (16)$$

Rearranging Eq. (16) and setting  $\chi = e^{b\gamma} \lambda^{1/\beta}$ , we get

$$(\chi - 1)\hat{\kappa}_l = 0, \quad (17)$$

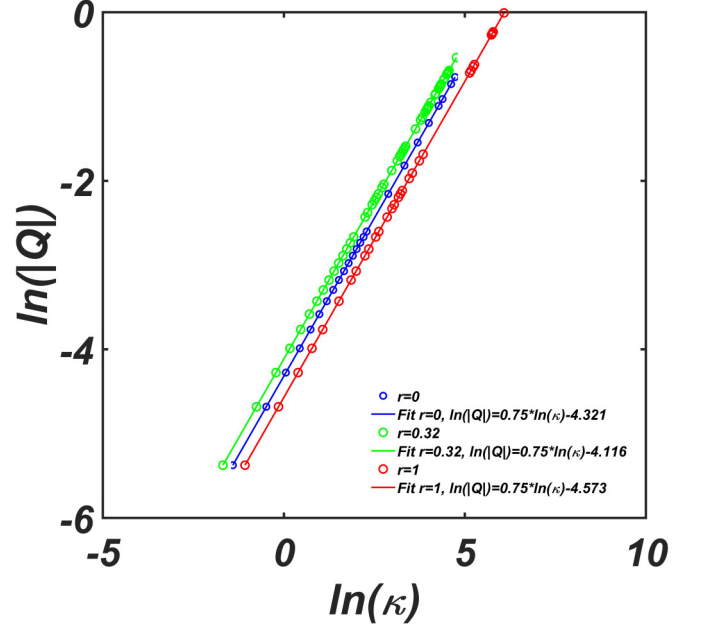


FIG. 8. Scaling relationship between flow and normalized edge conductivity. The data points from all the edges with conductivity value larger than  $10^{-8}$  are shown. The circles represent numerical data and the solid lines are fit. For  $r = 0$ , no control is applied, while  $r = 0.32$  specifies that 32% of the randomly chosen edges are subject to a control signal characterized by the parameter values  $\mu = 250$  and  $\sigma = 50$ . The control signals are fixed in time. For  $r = 1$ , each and every edge receives a control signal. All other parameters are the same as those in Fig. 3. As the final NGO network has 217 units, the number of edges with conductivity value larger than  $10^{-8}$  is 216.

which indicates  $\hat{\kappa}_l = 0$  for the steady state. Because there are at least  $n - 1$  edges with positive conductivity values, the quantity  $\hat{\kappa}_l$  can have values that are different from the steady state value. The only possibility to resolve the contradiction is  $\chi = e^{b\gamma} \lambda^{1/\beta} = 1$ , validating the flow-conductivity scaling law for the case of  $f(|Q_l|) = |Q_l|^\gamma$ .

In our simulations, the form of  $f(|Q_l|)$  is more complicated:  $f(|Q_l|) = |Q_l|^\gamma / (1 + h|Q_l|^\gamma)$ . We can argue that the algebraic flow-conductivity scaling law still holds. In particular, for  $t \rightarrow \infty$ , we have  $g(t, \mu) \rightarrow 0$ . The condition for the dynamics to reach the steady state is

$$|Q_l|^\gamma / (1 + h|Q_l|^\gamma) - \hat{\kappa}_l = 0. \quad (18)$$

Substituting the scaling relationship into this equation, we have:

$$\frac{\chi \hat{\kappa}_l}{1 + h\chi \hat{\kappa}_l} - \hat{\kappa}_l = 0 \quad (19)$$

or  $(\chi - 1 - h\chi \hat{\kappa}_l)\hat{\kappa}_l = 0$ . The condition under which a steady state has been reached is  $\hat{\kappa}_l = 0$ . For  $\chi \approx 1$ , we have  $\chi - 1 - h\chi \hat{\kappa}_l \approx 0$ , because  $h$  is a small quantity (e.g.,  $h = 0.001$ ) and  $\hat{\kappa}_l < 1$ , as explained in Sec. III E. While the argument is only approximate, it gives indication as to how the adaptive dynamical process can result in  $n - 1$  distinct conducting edges, providing a physical reason for the emergence of the scaling law between flow and conductivity.

### B. Nonmonotonic behavior of total dissipation

To obtain a physical understanding of the counterintuitive nonmonotonic behavior in the total dissipation versus the fraction of controlled edges, we begin by identifying the parameters on which the dissipation depends. Recall the definition of the total dissipation:

$$E = \sum_l D_l \frac{Q_l^2}{\kappa_l}. \quad (20)$$

Substituting the flow-conductivity scaling relationship,  $\ln(|Q_l|) = \ln(\kappa_l)/\gamma + b$ , into Eq. (20), we get

$$E = \sum_l D_l e^{2b} \kappa_l^{2/\gamma-1} = e^{2b} \sum_l D_l \kappa_l^{2/\gamma-1}. \quad (21)$$

For  $\gamma = 4/3$  and  $\beta = 1/2$ , we get  $E = e^{2b} \sum_l D_l \kappa_l^{1/2} = e^{2b} \text{const}$ , indicating that a large  $b$  value will lead to a higher value of the total dissipation. The steady-state condition in Sec. IV A, i.e.,  $\chi \approx 1$ , indicates that a smaller value of  $\lambda$  will lead to a higher value of  $b$ . Because of the relation  $\lambda = \text{const}/\sum_l D_l \hat{\kappa}_l^{1/2}$ , we have that a high value of  $\sum_l D_l \hat{\kappa}_l^{1/2}$  corresponds to a small value of  $\lambda$ . The intuition is then that, to have an NGO transportation network from the adaptive dynamics with  $\gamma = 4/3$  and  $\beta = 1/2$ , one should make the value of  $\sum_l D_l \hat{\kappa}_l^{1/2}$  as small as possible to satisfy the Kirchhoff's current law.

To test this result, we show in Fig. 9(a) the values of  $\hat{\kappa}_l^{1/2}$  and its accumulative value for all edges with conductivity larger than  $10^{-8}$  for the same network as in Fig. 8. Figure 9(b) shows that the accumulative value for  $r = 1$  for the edges with the largest conductivity values is larger than those for  $r = 0$  and  $r = 0.32$  prior to rank < 13. That is, among the three cases, the network for  $r = 1$  has the largest main vein. However, for rank > 13, the accumulative value for  $r = 0.32$  is larger than those for the other two cases. For rank > 95, the accumulative value for  $r = 0$  is larger than that for the  $r = 1$  case, indicating that the number of small conductivity edges for  $r = 0$  is larger than that for  $r = 1$ . Figure 9(a) reveals that the main vein for  $r = 0.32$  is longer than that for  $r = 1$ , leading to the highest total dissipation value for  $r = 0.32$  (among the three cases examined). In fact, for  $r = 0.32$ , there are relatively many more large conductivity edges for  $12 < \text{rank} < 96$ , as can be seen from the network structure in Fig. 3.

### C. Main factor determining total dissipation

The total dissipation, defined in Eq. (21), is associated with the steady state of the adaptive dynamics, where the following condition holds:

$$\chi = e^{b\gamma} \lambda^{1/\beta} \approx 1. \quad (22)$$

Replacing  $\kappa_l$  by  $\hat{\kappa}_l$  in Eq. (21), we obtain

$$E = e^{2b} \sum_l D_l (\lambda^{1/\beta})^{1/\gamma-1} \hat{\kappa}_l^{2/\gamma-1}, \quad (23)$$

indicating that the total dissipation depends on  $\gamma$  and  $\beta$  in a complicated manner. Combining Eqs. (23) and Eq. (22), we

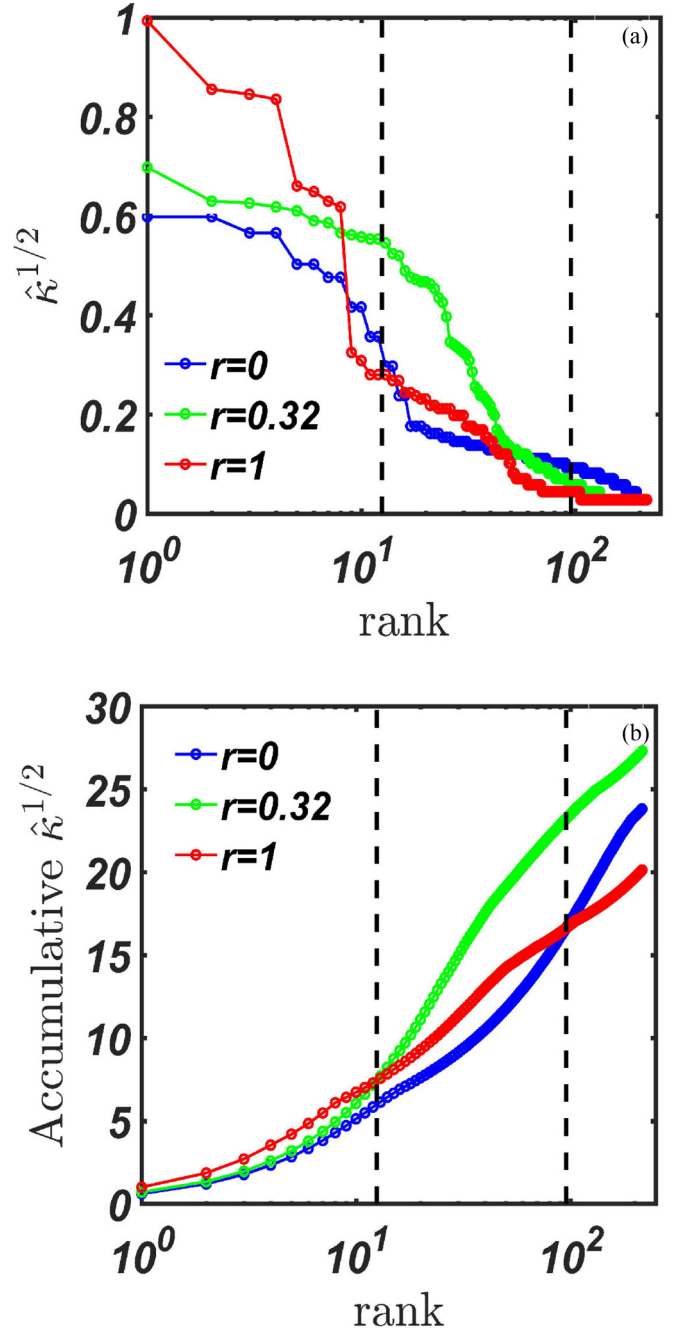


FIG. 9. Heuristic understanding of the nonmonotonic behavior of total dissipation versus the fraction of controlled edges. [(a) and (b)] The quantity  $\hat{\kappa}_l^{1/2}$  and its accumulative sum, respectively, for all edges with conductivity values larger than  $10^{-8}$ . Legends and parameter values are the same as those in Fig. 8. The results are arranged in terms of decreasing conductivity values. The black dashed line on the left side indicates that the value of  $\hat{\kappa}_l^{1/2}$  for  $r = 0.32$  is larger than those for  $r = 1$  and  $r = 0$ . The black dashed line on the right side shows that the accumulative value of  $\hat{\kappa}_l^{1/2}$  for  $r = 0$  is larger than that for  $r = 1$ .

get

$$E \approx \lambda^{1/\beta} \sum_l D_l \hat{\kappa}_l^{2/\gamma-1}. \quad (24)$$

Using the relation  $\lambda = \text{const}/\sum_l D_l \hat{\kappa}_l^\beta$  with  $\text{const} = \sum_l D_l 0.5^\beta$  in our system setting, we have

$$E \approx \frac{(\sum_l D_l \hat{\kappa}_l^\beta)^{1/\beta} (\sum_l D_l \hat{\kappa}_l^{2/\gamma-1})}{(\sum_l D_l 0.5^\beta)^{1/\beta}}. \quad (25)$$

To assess how the total dissipation depends on the feedback parameter  $\gamma$ , we set  $\beta = 1/2$  to obtain

$$E \approx \frac{(\sum_l D_l \hat{\kappa}_l^{0.5})^2 (\sum_l D_l \hat{\kappa}_l^{2/\gamma-1})}{(\sum_l D_l 0.5^{0.5})^2}. \quad (26)$$

As the value of  $\gamma$  is changed systematically, the total dissipation also changes continuously—there is no discontinuity. This means that the discontinuity in Fig. 7 must be due to the change in the structure of the transportation network as  $\gamma$  is changed, indicating a weak dependence of the dissipation on the feedback parameter.

Similarly, to understand the dependence of the total dissipation on the cost-limiting parameter  $\beta$ , we fix  $\gamma = 4/3$  to obtain

$$E \approx \frac{(\sum_l D_l \hat{\kappa}_l^\beta)^{1/\beta} (\sum_l D_l \hat{\kappa}_l^{0.5})}{(\sum_l D_l 0.5^\beta)^{1/\beta}}, \quad (27)$$

giving a sophisticated dependence of  $E$  on  $\beta$ . Numerically, we find that the dependence is relatively weak.

The heuristic analysis of the total dissipation on the parameters  $\gamma$  and  $\beta$  thus reveals a rather weak dependence, suggesting that the network structure has a predominate influence on the dissipation.

## V. DISCUSSION

Designing optimal transportation networks is relevant to applied science and engineering fields such as computer science and civil engineering in terms of specific systems such as computer networks, water supply networks, the power grids, and communication networks. Yet the basic physical mechanism and principle underlying the achievement of globally optimal networks remain elusive. For uncovering the dynamical origin of how a complex adaptive networked system can evolve into an optimal state, insights from natural systems, especially biological systems, are useful, as optimal transportation networks abound in plants and animals in nature. However, because of our limited understanding of the working of these natural systems, biologically inspired adaptive dynamics-based design can fail to yield even NGO networks [26]. Recognizing that external driving is crucial for growth in biological systems [30], we articulate and investigate the idea of incorporating control into biologically inspired adaptive dynamics for generating NGO transportation networks.

We introduce a general class of sigmoid functions (similarly to Fermi-Dirac distribution in statistical physics, which has been widely used in various areas of complex dynamical systems) as the control signal, whose strength gradually decays with time evolution of the adaptive dynamics. We find that partial control, i.e., applying control signals to only a fraction of the edges in the network, can generate unexpectedly high total dissipation, as represented by a counterintuitive, nonmonotonic behavior of the dissipation in its dependence

on the fraction of the controlled edges. We have provided a heuristic explanation for the nonmonotonic behavior. Importantly, we find that, with certain temporal control strategy, there exist optimal control signals of small amplitudes that can eliminate this undesired nonmonotonic behavior and lead to NGO transportation networks. In particular, the key ingredient of our control strategy is being “temporal” in the sense that we do not choose a fixed set of edges for control but randomly switch the set of the same size from time to time. The temporal variation in the control set, coupled with targeting the edges with small conductivity values, can yield NGO transportation networks, regardless of system details such as the initial network structure and values of the system parameters. While we can find the NGO transportation networks by varying the control set of edges, at the present there is no first-principle method that can be used to identify the set of minimum control links so as to generate NGO transportation networks in a self-consistent manner.

Our work broadens, significantly, the ways to design NGO transportation networks by exploiting both biologically inspired adaptive dynamics and control. This, in principle, can generate an infinite number of distinct NGO networks (the cases demonstrated in this paper are only a small set of illustrative examples). This is consistent with the proclaim of prominent mathematician and philosopher Gottfried W. Leibniz: “There are no two identical leaves in the world.” Indeed, the fact that there exist different leaf vein structures indicates that they all belong to the NGO type. Thus, while there are no two identical leaves in the world, we find the following claim appropriate to conclude this paper: All the leaves have an NGO structure.

## ACKNOWLEDGMENT

We acknowledge support from the Vannevar Bush Faculty Fellowship program sponsored by the Basic Research Office of the Assistant Secretary of Defense for Research and Engineering and funded by the Office of Naval Research through Grant No. N00014-16-1-2828.

## APPENDIX: EFFECTS OF TISSUE SHAPE AND DISORDERED COARSE-GRAINED GRID

To address the issue of whether variations in the tissue shape would affect the ability of the evolutionary dynamics to yield an NGO transportation network, for simplicity we consider the setting where a control signal is applied to each and every edge and study three combinations of the tissue shape and lattice structure. The results are shown in Fig. 10. Specifically, shown in Figs. 10(a), 10(b) and 10(e) are the final transportation networks resulting from a leaf-shaped tissue, from such a tissue with a disordered coarse-grained grid, and from a circular tissue, respectively. The corresponding time evolution of the total dissipation is shown in Figs. 10(c), 10(d) and 10(f), respectively, which exhibit a similar pattern. The tissues in Figs. 10(a) and 10(e) have a triangular lattice structure and all resulting networks are of the NGO type. The results suggest that the tissue shapes and lattice structure have no effect on the ability for a fully controlled system to evolve into a transportation network of the NGO type.

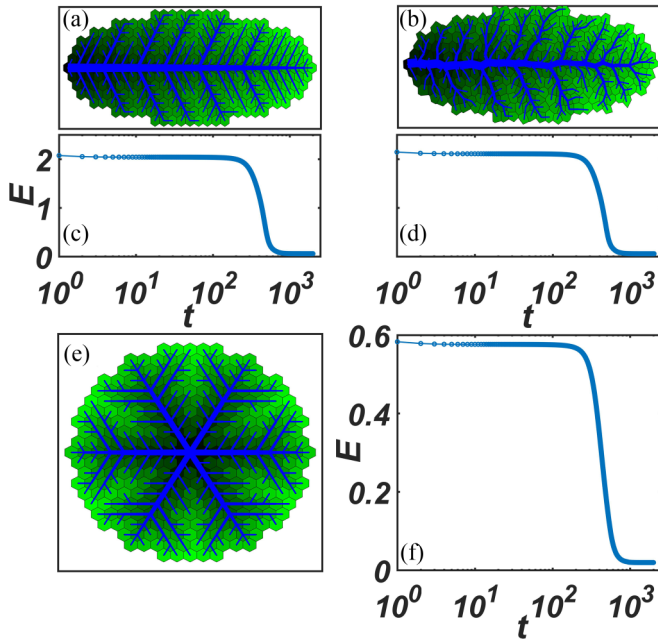


FIG. 10. NGO transportation networks resulted from different tissue shapes and disordered coarse-grained grids. All edges receive a control signal. [(a), (b), and (e)] NGO transportation networks obtained from a leaf-shaped tissue with a triangular lattice structure, a leaf-shaped tissue with a disordered coarse-grained grid, and a circular shape tissue with a triangular lattice structure, respectively. [(c), (d), and (f)] Time evolution of the total dissipation corresponding to the cases in (a), (b), and (e), respectively. The optimal transportation networks in panels (a), (b), and (e) have total dissipation  $E = 0.060704$ ,  $E = 0.059422$ , and  $E = 0.019519$ , respectively. In all cases, the evolution time is 2000 time steps, and the control parameter is  $\mu = 250$ . For the leaf-shaped tissue, there are  $n = 291$  units and  $m = 802$  edges. For the circular-shaped tissue, there are  $n = 301$  units and  $m = 840$  edges. Other parameters are the same as in Fig. 3 in the main text.

When partial control is applied, NGO transportation networks can still arise, as shown in Fig. 11, where the tissue shapes and lattice structure are the same as those in Fig. 10. For a leaf-shaped tissue with a triangular lattice structure, partial control does not affect the total dissipation associated with the final NGO network [cf. Fig. 10(a) and Fig. 11(a)]. However, when a disordered coarse-grained grid is used, partial control results in a higher amount of the total dissipation,

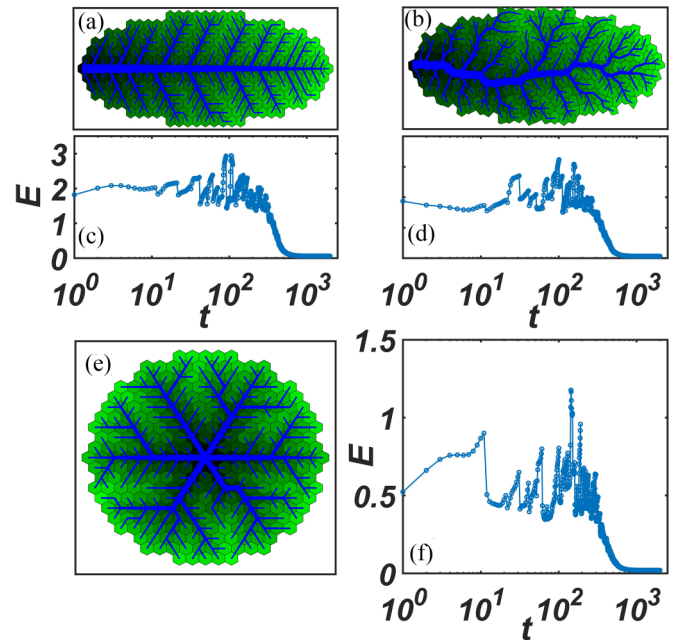


FIG. 11. NGO transportation network from different tissue shapes and coarse-grained grid under partial control. The scheme is to apply a control signal to 50% of randomly chosen edges for  $T_0 = 10$ . [(a), (b), and (e)] The final NGO transportation networks (after 2000 time steps) from a leaf-shaped tissue with a triangular lattice structure, such a tissue with disordered coarse-grained grid, and a circular tissue with a triangular lattice structure, respectively. [(c), (d), and (f)] The corresponding time evolution of the total dissipation. The optimal transportation networks in panels (a), (b), and (e) have total dissipation  $E = 0.060653$ ,  $E = 0.064113$ , and  $E = 0.019645$ , respectively. The strength of the control signal is  $\mu = 250$ . Other parameters are the same as those in Fig. 10.

as shown in Fig. 11(b), which is about 8% higher than that under full control. The reason is that, under partial control, the main vein tends to bend. For a circular tissue with a triangular lattice structure, partial control results in a final NGO network with a more complicated structure with slightly more total dissipation in comparison with the case of full control, as shown in Figs. 11(e) and 11(f). We find that using a different value of the strength of the control signal (e.g.,  $\mu = -250$ ) or targeting a set of edges with small conductivity can result in qualitatively similar NGO networks.

- [1] N. Wieberneit, Service network design for freight transportation: A review, *OR Spec.* **30**, 77 (2008).
- [2] S. V. Ukkusuri, T. V. Mathew, and S. T. Waller, Robust transportation network design under demand uncertainty, *Comp. Aided Civ. Inf.* **22**, 6 (2007).
- [3] R. Z. Farahani, E. Miandoabchi, W. Y. Szeto, and H. Rashidi, A review of urban transportation network design problems, *Eur. J. Oper. Res.* **229**, 281 (2013).
- [4] M. Pternea, K. Kepaptsoglou, and M. G. Karlaftis, Sustainable urban transit network design, *Tran. Res. A* **77**, 276 (2015).
- [5] D. Morgan and I. Goulter, Optimal urban water distribution design, *Water Resour. Res.* **21**, 642 (1985).
- [6] P. K. Swamee and A. K. Sharma, *Design of Water Supply Pipe Networks* (John Wiley & Sons, New York, 2008).
- [7] A. Rinaldo, R. Rigon, J. R. Banavar, A. Maritan, and I. Rodriguez-Iturbe, Evolution and selection of river networks: Statics, dynamics, and complexity, *Proc. Natl. Acad. Sci. USA* **111**, 2417 (2014).
- [8] L. Cheng and B. W. Karney, Organization and scaling in water supply networks, *Phys. Rev. E* **96**, 062317 (2017).

- [9] A. E. Motter and Y.-C. Lai, Cascade-based attacks on complex networks, *Phys. Rev. E* **66**, 065102(R) (2002).
- [10] S. V. Buldyrev, R. Parshani, G. Paul, H. E. Stanley, and S. Havlin, Catastrophic cascade of failures in interdependent networks, *Nature* **464**, 1025 (2010).
- [11] J. R. Banavar, F. Colaiori, A. Flammini, A. Maritan, and A. Rinaldo, Topology of the Fittest Transportation Network, *Phys. Rev. Lett.* **84**, 4745 (2000).
- [12] V. Colizza, J. R. Banavar, A. Maritan, and A. Rinaldo, Network Structures from Selection Principles, *Phys. Rev. Lett.* **92**, 198701 (2004).
- [13] S. Bohn and M. O. Magnasco, Structure, Scaling, and Phase Transition in the Optimal Transport Network, *Phys. Rev. Lett.* **98**, 088702 (2007).
- [14] M. Durand, Structure of Optimal Transport Networks Subject to a Global Constraint, *Phys. Rev. Lett.* **98**, 088701 (2007).
- [15] E. Katifori, G. J. Szöllösi, and M. O. Magnasco, Damage and Fluctuations Induce Loops in Optimal Transport Networks, *Phys. Rev. Lett.* **104**, 048704 (2010).
- [16] F. Corson, Fluctuations and Redundancy in Optimal Transport Networks, *Phys. Rev. Lett.* **104**, 048703 (2010).
- [17] T. Gavrilchenko and E. Katifori, Resilience in hierarchical fluid flow networks, *Phys. Rev. E* **99**, 012321 (2019).
- [18] J. Strake, F. Kaiser, F. Basiri, H. Ronellenfitch, and D. Witthaut, Non-local impact of link failures in linear flow networks, *New J. Phys.* **21**, 053009 (2019).
- [19] P. S. Stevens, *Patterns in Nature* (Little, Brown & Co., New York, 1974).
- [20] P. Ball and N. R. Borley, *The Self-Made Tapestry: Pattern Formation in Nature* (Oxford University Press, Oxford, 1999), Vol. 198.
- [21] E. Bertuzzo, F. Carrara, L. Mari, F. Altermatt, I. Rodriguez-Iturbe, and A. Rinaldo, Geomorphic controls on elevational gradients of species richness, *Proc. Natl. Acad. Sci. USA* **113**, 1737 (2016).
- [22] B. Blonder, C. Violle, L. P. Bentley, and B. J. Enquist, Venation networks and the origin of the leaf economics spectrum, *Ecol. Lett.* **14**, 91 (2011).
- [23] L. Papadopoulos, P. Blinder, H. Ronellenfitch, F. Klimm, E. Katifori, D. Kleinfeld, and D. S. Bassett, Comparing two classes of biological distribution systems using network analysis, *PLoS Comp. Biol.* **14**, e1006428 (2018).
- [24] E. Katifori, The transport network of a leaf, *C. R. Phys.* **19**, 244 (2018).
- [25] M. Durand, Architecture of optimal transport networks, *Phys. Rev. E* **73**, 016116 (2006).
- [26] A. Tero, S. Takagi, T. Saigusa, K. Ito, D. P. Bebbler, M. D. Fricker, K. Yumiki, R. Kobayashi, and T. Nakagaki, Rules for biologically inspired adaptive network design, *Science* **327**, 439 (2010).
- [27] A. Tero, R. Kobayashi, and T. Nakagaki, A mathematical model for adaptive transport network in path finding by true slime mold, *J. Theor. Biol.* **244**, 553 (2007).
- [28] X. Zhang, A. Adamatzky, F. T. Chan, Y. Deng, H. Yang, X.-S. Yang, M.-A. I. Tsompanas, G. C. Sirakoulis, and S. Mahadevan, A biologically inspired network design model, *Sci. Rep.* **5**, 10794 (2015).
- [29] D. Hu and D. Cai, Adaptation and Optimization of Biological Transport Networks, *Phys. Rev. Lett.* **111**, 138701 (2013).
- [30] H. Ronellenfitch and E. Katifori, Global Optimization, Local Adaptation, and the Role of Growth in Distribution Networks, *Phys. Rev. Lett.* **117**, 138301 (2016).
- [31] T. Nakagaki, M. Iima, T. Ueda, Y. Nishiura, T. Saigusa, A. Tero, R. Kobayashi, and K. Showalter, Minimum-Risk Path Finding by an Adaptive Amoebal Network, *Phys. Rev. Lett.* **99**, 068104 (2007).
- [32] A. Takamatsu, T. Gomi, T. Endo, T. Hirai, and T. Sasaki, Energy-saving with low dimensional network in physarum plasmodium, *J. Phys. D: Appl. Phys.* **50**, 154003 (2017).
- [33] See Supplemental Material at <http://link.aps.org/supplemental/10.1103/PhysRevE.100.032309> for representative time evolution of the transportation network towards a nearly optimal structure.
- [34] F. Simini, A. Rinaldo, and A. Maritan, Universal scaling of optimal current distribution in transportation networks, *Phys. Rev. E* **79**, 046110 (2009).
- [35] A. Maritan, F. Colaiori, A. Flammini, M. Cieplak, and J. R. Banavar, Universality classes of optimal channel networks, *Science* **272**, 984 (1996).